AIAA JOURNAL
Vol. 47, No. 4, April 2009

Control of Particle Damper Nonlinearity

C. Wong* and J. Rongong†
University of Sheffield, Sheffield, England S1 3JD, United Kingdom

DOI: 10.2514/1.38795

A particle damper comprises granular material enclosed in a container that is attached to or within a vibrating structure. Vibration is suppressed by the particle damper by a combination of friction, inelastic collisions, and kinetic energy storage. The principal challenges are that their performance is highly nonlinear and is dependent on many parameters. Although significant efforts have been made to characterize and model particle dampers, there is very little evidence of efforts made to tune or control their nonlinear behavior effectively. The research work carried out in this project is based on the supposition that the granular state within the damper can be altered in a predictable way to ensure that one operates in a zone where damping is high. This work shows that this can be achieved by altering the static effective pressure in the granular system. A variety of physical embodiments were considered (including magnetic fields and airbags): the design features sought were simplicity, uniform pressure distribution, and ease of automation. The final configuration selected was a thick layer of polyurethane foam that could be pressed down onto the particles with various pressures, depending on the tightness of the screw-top lid. A second set of energy loss estimates is also obtained by running the discrete element modeling prediction for the damper using appropriate interactions models. Results are finally compared with those obtained from physical experiments.

Nomenclature

c_n	=	normal viscous damping coefficient
c_s	=	shear viscous damping coefficient
c_{sky}	=	skyhook damper viscous damping coefficient
$\mathbf{F}_i$	=	resultant force vector on a particle
$\mathbf{F}_n$	=	normal force vector on particle
f	=	measured force from power dissipation experiment
g	=	gravity acceleration constant
$\mathbf{g}_i$	=	body acceleration vector (e.g., gravity)
k_{foam}	=	linearized stiffness of foam wall
k_n	=	effective normal stiffness
k_{ni}	=	normal stiffness of the ith entity
k_s	=	effective shear stiffness
k_{si}	=	shear stiffness of the ith entity
m	=	mass of a particle
m_{eff}	=	effective mass of a particle damper
m^*	=	effective mass of two contacting particles
P_{foam}	=	estimated power dissipated by foam
R	=	particle radius
v	=	measured velocity from power dissipation experiment
x_i	=	position of particle
Y_i	=	yield stress of the ith entity
α	=	coefficient of restitution
Δt	=	time step
δ	=	particle penetration depth through the foam wall
δ_c	=	amount displacement of foam compressed
ζ	=	critical damping ratio
μ	=	coefficient of friction
ω	=	angular velocity
ω_0	=	fundamental harmonic frequency

Presented as Paper 2103 at the 49th AIAA/ASME/ASCE/AHS/ASC Structures, Structural Dynamics, and Materials Conference, Schaumburg, IL, 7–10 April 2008; received 28 May 2008; revision received 9 January 2009; accepted for publication 16 January 2009.

*Research Associate, Department of Mechanical Engineering, Mappin Street. Member AIAA.

†Lecturer, Department of Mechanical Engineering, Mappin Street. Member AIAA.

I. Introduction

A PARTICLE damper comprises granular material enclosed in a container that is attached to or within a vibrating structure. Vibration energy is dissipated by the damper through inelastic collisions and friction between particles. Energy is also stored within the damper in the form of kinetic energy and strain energy of the particles, giving the particle damper an effective mass.

The advantage of a particle damper is that it can be designed in such a way that it is invariant to temperature. This allows it to be used in harsh environments where traditional methods fail. It can also damp vibrations over a broad range of frequencies and can be implemented rather cheaply. Although the idea of adding mass into a structure to suppress vibration may seem like a way to mask bad design methodology, it can actually reduce the overall mass of the structure. This can be achieved by incorporating the particle dampers into the structure during the design process.

The combination of the effective mass and the energy dissipation mechanisms enables the particle damper to be used as an effective vibration suppression solution. This effect can be demonstrated in the dynamic behavior of a single-degree-of-freedom (SDOF) system (refer to Fig. 1). The vibrating mass of this SDOF system is basically an enclosure filled with particles. The dashed line in Fig. 1 shows the frequency response function (FRF) of the response amplitude to the force amplitude. When the enclosure is filled with particles, the curve shifts to curve 1 for a low-force excitation (all subsequent curve numbers from 1–11 correspond to increasing excitation amplitude [1]). The shift is due to a drop in natural frequency caused by the increased mass in the SDOF system. As the excitation force is increased, the curve shifts downward (as in curve 2). The reduced response indicates an increased level of damping in the system, as the particles collide and rub against one another more effectively. The natural frequency, however, shifts upward instead of downward, as opposed to conventional viscous damping. This is due to a drop in the effective mass seen by the system as the contact time between the particles and the walls of the enclosures is reduced.

As the amplitude is further increased, the observed damping level increases concurrent with reductions in the effective mass of the system. This goes up to the amplitude levels of between curves 4 and 5, where the optimum level of damping seems to have been achieved. The damping levels, however, start to decrease as the amplitude of excitation is increased further and the effective mass starts to approach the mass of the casing itself.

Without much loss in generality, the conceptual lumped parameter model of a SDOF system with a particle damper can be visualized in Fig. 2. It can be seen that the particle damper acts almost like a

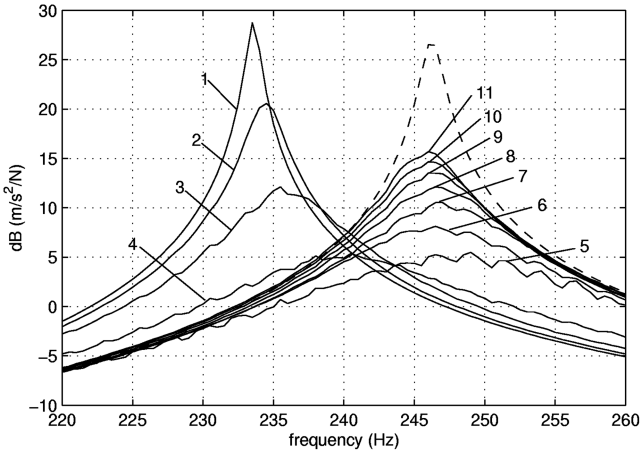

Fig. 1 Frequency response function of a SDOF system with an empty enclosure as the vibrating mass (dashed line) and with particles filled into the vibrating mass (solid lines). Each curve is of different amplitudes [1].

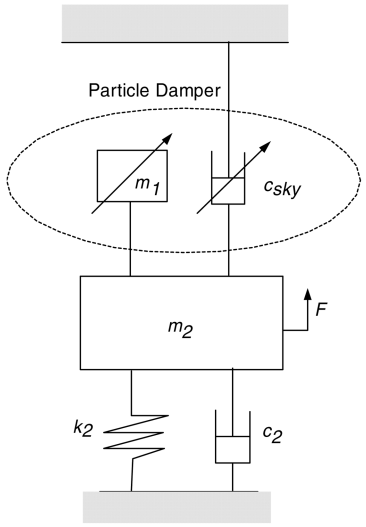

Fig. 2 Lumped parameter model of particle damper attached to a SDOF system.

combination of a tuned mass damper (where energy is transferred away from the structure that is to be protected into the kinetic energy and strain energy of the mass damper) and a skyhook damper (where damping is dependent on absolute motion instead of relative motion). In the case of the particle damper, the strain and kinetic energy is assumed trapped as kinetic energy only. This is encapsulated in the effective mass of the system. Both the effective mass of the damper m_1 and the damping coefficient of the skyhook damper c_{sky} are functions of vibration amplitude and frequency for a particular configuration.

The principal challenge in particle damper design is the large amount of parameters to tune to achieve a particular level of performance. The geometry and material of the enclosure, the particle material, the size distribution of the particles, and geometry of the particles are just some of the parameters that play a role in the capability of the damper. This is further complicated by the nonlinear dependence of the power trapped and dissipated in the particle damper to amplitude and frequency. This complex variable behavior is also one of the strong points of particle dampers, as it allows the designer a great deal of flexibility in achieving a desired performance. To further extend the degree of variability, a field of force can be applied to the particles (such as filling the enclosures with liquid or applying an electromagnetic field [2], leading to a semi-active particle damper).

The best way to control the particle damper performance, however, requires an in-depth understanding of how the particle assembly itself behaves. An attempt to explain the damping behavior of granular materials is by the use of the three-phase map [3,4]. The phase map shows that, depending on the vibration amplitude and frequency, the behavior of polydisperse (particles of a certain distribution of diameter) granular media can approximate a solid, liquid, or gas. The level of energy dissipation in each "phase" is very different. The research work carried out in this paper is based on the supposition that this "phase map" can be altered in a predictable way to ensure that one operates in a zone where damping is high. Although moderately high energy dissipation has been reported for the gaslike phase (dominated by inelastic collisions), it is thought that the most effective dissipation is achieved when the granular medium is still in the solidlike phase, close to, but not at, the point where particles roll over each other, demonstrating convective patterns. Although convective patterns are not always observed in particle dampers (mostly those that have one fixed particle diameter, e.g., [5,6]), it hints at the fact that dissipation by friction may be a dominant mechanism. This is so because convective patterns indicate that the particles are rolling over one another, instead of a shearing contact between the particles. The dominance of friction has also been reported from discrete element modeling (DEM) simulations [6].

The role of static pressure has been suggested as one factor that affects the state of the granular media during vibration. Changes in amplitude dependence for dampers of different shapes have been explained by considering the static pressure [1]. For a damper used in practice, the key ability required is to be able to alter the position of the phase map effectively to ensure that peak damping (in the "solid" zone) occurs around the operating point. This work shows that this can be achieved by altering the static effective pressure in the granular system. Other related methods of preloading the particles have also been attempted in the past. An example of this is the use of a beanbag damper to damp the vibrations of a ski [7]. A variety of physical embodiments were considered for this work (including magnetic fields and airbags; the design features sought were simplicity, uniform pressure distribution, and ease of automation). The final configuration selected was a thick layer of open cell polyurethane (PU) foam that could be pressed down onto the particles with variable stiffness depending on the tightness of the screw-top lid. A second set of energy loss estimates are then obtained by running the DEM prediction for the damper using appropriate interactions models. Results are finally compared with those obtained from physical experiments.

The layout of the paper is as follows. Section II relates the different experiments performed to estimate the energy dissipation and effective mass of the particles. Section III details the contact models and simulation variables used in the DEM simulation. The paper is concluded in Sec. IV.

II. Experimental Method

A. Power Measurements

To characterize the effective mass and energy dissipation, power measurement tests were performed on the particle damper. This is based on the Fourier-based power flow method that Yang [5] used to characterize particle dampers. Basically, the complex power of the damper during vibration is measured from the force and velocity signals of the damper. The complex power can be easily acquired from experiments via the cross-spectrum calculation built into most signal analyzers. The complex power spectrum for the nth harmonic is given as

$$P_n = f_{n,\text{rms}} v^*_{n,\text{rms}} \tag{1}$$

where $f_{n,\text{rms}}$ denotes the Fourier transform of the force normalized to its root-mean-square level (dividing the magnitude by $\sqrt{2}$), whereas $v^*_{n,\text{rms}}$ is the conjugate of the Fourier transform of the velocity normalized to its root-mean-square level. The total complex power P_{complex} is the sum of the complex power spectrum over all the harmonics:

$$P_{\text{complex}} = \sum_n P_n \tag{2}$$

It is possible to perform the same power measurements for any signals using this method, provided that it is a periodic signal. Vibration damping, however, is usually analyzed within single resonances. Therefore, analysis in this work has been restricted to the use of single harmonics. This would result in analysis being restricted to Eq. (1). For complicated structures with multiple resonances, the analysis may be repeated to account for the different resonances.

The average dissipated power (also known as active power) can be extracted from the real part of the complex power. The imaginary part of Eq. (2) corresponds to a term usually known as reactive power. Reactive power is conventionally interpreted physically as the maximum power stored in the system. The derivation of reactive power comes from the phasor difference between apparent power (the product of root mean square of force with the root mean square of velocity) and active power.

Assuming that the stored energy is in the form of kinetic energy, one could also calculate an effective mass m_{eff} that is associated with the particle damper:

$$m_{\text{eff}} = \frac{2 \cdot \text{Im}\{P_n\}}{n\omega_0 v_{n,\text{rms}}^2} \tag{3}$$

where ω_0 is the fundamental frequency.

B. Experiment Setup

A Perspex particle damper was chosen for the characterization procedure. This is similar in construction to the particle damper used by Yang [5]. The particle damper consists of a cylindrical casing with a screw-top lid and a securing ring. An open-cell PU foam of 1-cm thickness is placed in between the bottom of the screw-top lid and the top of the particles. The screw-top lid allows the compression of the foam, leading to a variable stiffness due to the nonlinear property of the foam. The foam is in contact with the screw-top lid and the top layer of particles at all times. The transparent casing also allows one to view the movement of the particles during the operation of the damper. A schematic of the particle damper casing is shown in Fig. 3.

The physical experiments involve mounting the Perspex damper onto an electromagnetic shaker (refer to Fig. 4). The connection between the damper and the shaker is buffered by a force transducer, while the response of the damper is measured with an accelerometer. The analysis was deliberately restricted to 225 stainless steel ball bearings 3 mm in diameter for all tests, to simplify the modeling aspect. The static mass of the casing is 104.7 g, the combined mass of the particles is 22.24 g, and the mass of the foam is 0.32 g. This leads to an overall static mass of 127.26 g.

Four different sets of experiments were conducted to characterize the damper: when the foam is uncompressed, when it is compressed by 1.5 mm, by 4 mm, and by 6 mm. Each set of experiments was performed for a range of vertical excitation stepped sine tests for frequencies from 25 to 225 Hz, in increments of 20 Hz, and for a range of amplitudes from 5 to 17 g, in increments of 2 g (except for the uncompressed foam configuration as the particles are lodged to the side of the foam for amplitudes above 13 g).

Because the acceleration was measured instead, the measured cross spectrum from the experiments was integrated in the frequency domain to recover the correct values. There was also a lag between the two signals that was not a property of power loss. This is more of an electronic phase error of the signals. This problem was also encountered by Yang [5] and should be compensated for, to avoid potential large measurement errors. One only has to perform the power measurement experiment with an empty particle damper casing and take note of the phase lag. This phase should be added to the phase difference of subsequent experiments with the particles.

The results of the experiments can be seen in Figs. 5 and 6. In the uncompressed foam configuration (Fig. 5a), the peak of power dissipation occurs around 45 Hz with 0.81 W dissipated at 13 g. A noticeable shift in the peak of power dissipation is observed as the

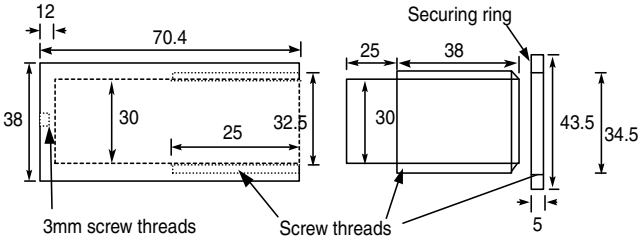

Fig. 3 Schematic of the particle damper casing.

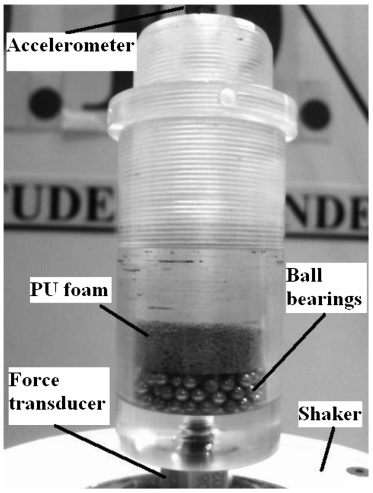

Fig. 4 Power measurements experimental setup.

foam is compressed. When it is compressed by 1.5 mm (15% static strain), the peak of power dissipation begins to move toward the higher frequencies. The peak power dissipation in this configuration is now at 55 Hz with 1.29 W dissipated at 17 g. At 13 g and 55 Hz, the peak power dissipation is almost at the same level of power dissipation as the peak of the uncompressed foam (0.80 W). As we increased the level of compression further to 4 mm (40% static strain), the peak shifts even further toward the higher frequency. The peak now occurs at 65 Hz, with a moderate decrease in power dissipation to 1.09 W at 17 g. The peak, however, is more rounded, indicating a better spread of power dissipation over a wider range of frequencies. The most drastic change, however, occurs when the foam is compressed by up to 6 mm (60% static strain). This reduces the peak of power dissipation significantly, down to 0.40 W at 17 g at 75 Hz. The average level of power dissipation for the higher frequencies has also increased. A possible explanation for the frequency shift for peak power dissipation is the nonlinearity of the foam. When the foam is compressed, the effective stiffness of the foam increases. The mass of the particle assembly and the foam behaves like a SDOF system, where higher stiffness leads to a shift of the resonance toward the higher frequency. By compressing the foam, the particles will also be constrained in a lower volume of mobility, leading to decreased levels of inelastic work done in collisions and possibly reduced shearing between the particles. Attention is drawn to the "kink" in the power dissipation curve for all levels of amplitudes for excitations of 85 and 95 Hz. This kink is thought to be the manifestation of the electronic phase error mentioned earlier. It was earlier assumed that the electronic phase errors are amplitude and frequency independent. Therefore, calibration was performed by only considering the average phase errors encountered at 25 Hz for a few levels (2–5 g) of excitation. These errors, however, seem to only occur at 85–95 Hz, resulting in a higher level of power dissipation than expected. Nevertheless, these errors are minor and do not detract from the overall results.

Focus is now brought to the effective mass of the system (refer to Fig. 6). The kink that was mentioned previously is also present in the calculation of the effective mass, leading to higher estimates. In fact,

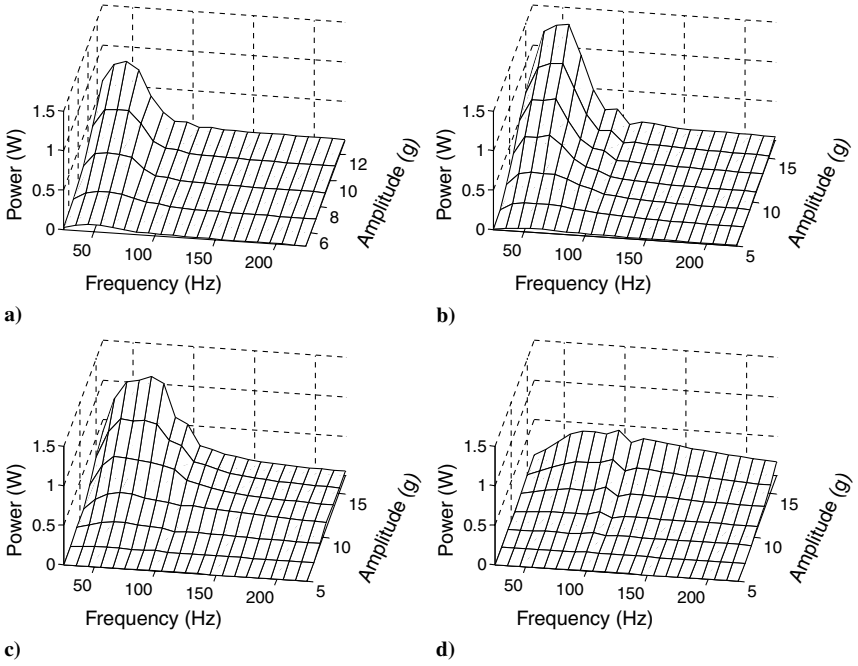

Fig. 5 Power dissipated measured for a) uncompressed foam, b) foam compressed by 1.5 mm, c) foam compressed by 4 mm, and d) foam compressed by 6 mm.

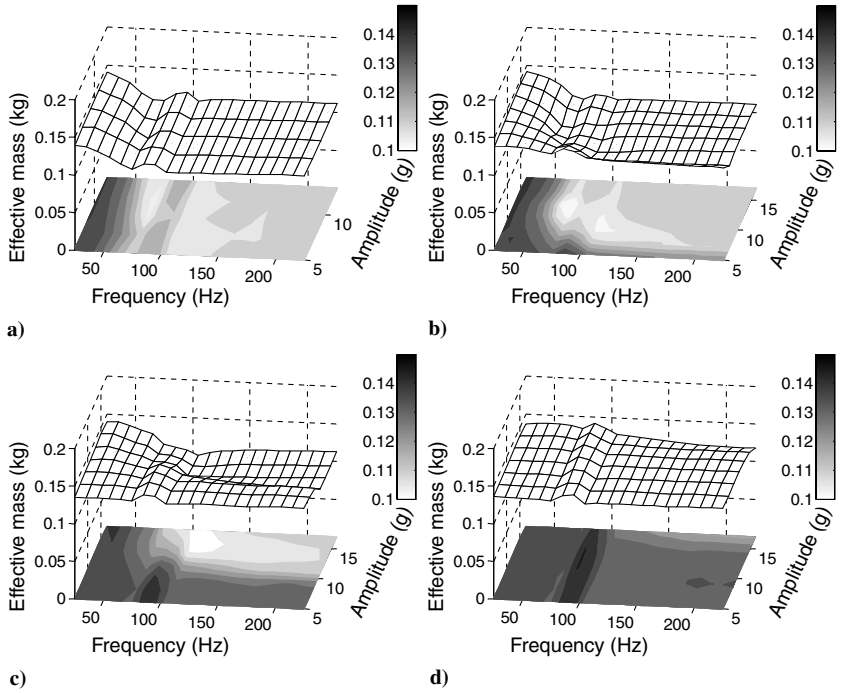

Fig. 6 Effective mass measured for a) uncompressed foam, b) foam compressed by 1.5 mm, c) foam compressed by 4 mm, and d) foam compressed by 6 mm.

it is more prevalent in the effective mass calculations than it is in the power dissipation curves. It is, however, quite easy to approximate the "correct" levels from a visual inspection of the curves. This can be done by doing a nearest-neighbor linear interpolation at the operating point, using the power dissipation values of the adjacent frequencies. Therefore, it is not a serious issue and can be ignored for now. When the foam is uncompressed, the effective mass of the overall damper is slightly higher than the static mass of the casing itself for almost all amplitudes above 50 Hz. It is interesting to note, however, that the effective mass below 50 Hz is actually higher than the static mass of the overall damper. This above-static mass property continues to appear for all four configurations, with increasing prominence at the lower levels of frequencies and excitation amplitude. In fact, when the foam is compressed up to 6 mm (60% strain), the effective mass for all operating points is higher than the static mass.

This combined particle damper foam is an illustration that damping can be effectively controlled by this simple mechanism. To gain better insight into the workings of the particle assembly in this configuration, a model of the damper is constructed using DEM. This shall be explained in the next section.

III. Discrete Element Method

A. Theoretical Aspect

The three-dimensional discrete element method used here is based on the commercial software, Particle Flow Code in 3 Dimensions (PFC3D) 3.1 [8]. The details of the method can be found in [9]. A brief review is reproduced here. In this implementation, all the particles are assumed to be perfect spheres (although clumps can be bonded together to form irregular particles). The particles and walls are also assumed to be rigid (rigid in the sense that the geometry does not warp for the purpose of calculations), and the particle displacement and contact area small relative to the particle sizes.

The equations of motion are applied for each particle, based on the resultant force and resultant moment on each particle. Laws of motion are not applied to the walls in the simulation. The motion of walls, however, is explicitly controlled using a specified wall velocity as an input. Assuming all the particles are of the same type and size, the equations of motion for the ith particle in vector form are given as

$$\mathbf{F}_i = m(\ddot{x}_i - g_i) \tag{4}$$

$$M_i = (\tfrac{2}{5}mR^2)\dot{\omega}_i \tag{5}$$

where $\mathbf{F}_i$ is the resultant force vector, m is the mass of a particle, x_i is the position of the particle, $\mathbf{g}_i$ is the body acceleration vector (e.g., gravity), R is the particle radius (1.5 mm for this particular paper), M_i is the resultant moment, and ω_i is the vector velocity. Given the resultant forces and moments, the position of the particle in one time step Δt is updated based on the equation

$$x_i^{(t+\Delta t)} = x_i^{(t)} + \dot{x}_i^{(t+\Delta t/2)}\Delta t \tag{6}$$

where the midinterval quantities are computed based on a centered finite difference scheme of the velocities

$$\dot{x}_i^{(t+\Delta t/2)} = \dot{x}_i^{(t-\Delta t/2)} + \left(\frac{\mathbf{F}_i^{(t)}}{m} + \mathbf{g}_i\right)\Delta t \tag{7}$$

$$\omega_i^{(t+\Delta t/2)} = \omega_i^{(t-\Delta t/2)} + \left(\frac{5M_i^{(t)}}{2mR^2}\right)\Delta t \tag{8}$$

For a multiparticle system, a critical time-step value is chosen automatically at each iteration. The critical time step is related to the highest natural frequency in the system. To perform a global eigenvalue analysis of the system is expensive. Therefore, a simplified approach is used to estimate the critical time step. A simple analysis of an uncoupled multi-degree-of-freedom system of linear springs and masses lead to a critical time step

$$t_{\text{crit}} = \min\left\{\begin{array}{l}\sqrt{m/k^{\text{tran}}} \\ \sqrt{I/k^{\text{rot}}}\end{array}\right. \tag{9}$$

where I is the moment of inertia, k^{tran} is the highest effective translational stiffness, and k^{rot} is the highest effective rotational stiffness calculated for all degrees of freedom for every particle. The time step chosen in simulation is actually the critical time step multiplied with a safety factor. The safety factor is fixed at 0.8 in this work.

The force acting on the particles comes from a combination of contact forces. A variety of contact models can be chosen to represent the contacts. In the pursuit of simplicity and expediency, linear spring and viscous damper contact models with Coulomb sliders were chosen. The formulation of this model and the extraction of the parameter values from experiments have already been discussed in [10]. It is noted that using this model reduces instability problems that may occur from the critical time-step calculations for nonlinear stiffness models [6]. A diagram of the contact models for different collisional conditions is shown in Fig. 7. The stiffness of the contacting entities is actually the effective stiffness (equivalent spring for two springs connected in series).

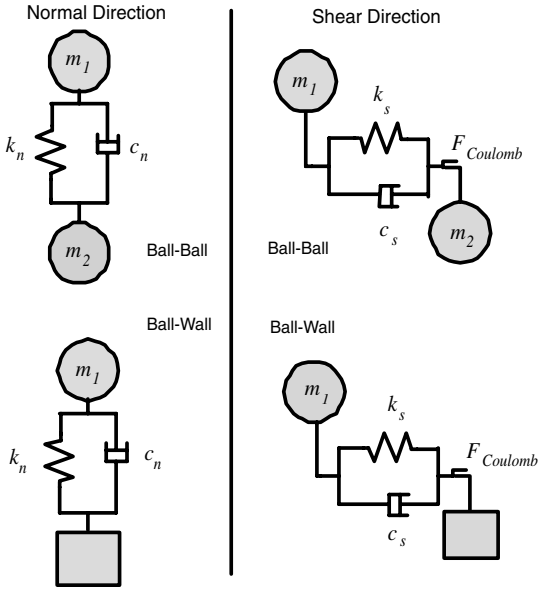

Fig. 7 Contact models used for different collision cases.

The normal stiffness of every ith entity is given as

$$k_{ni} = \frac{5.5}{4}\pi Y_i R \tag{10}$$

where Y_i is the yield stress of the ith entity. The shear stiffness of every ith entity is given as

$$k_{si} = \frac{3.3}{(1+\nu_i)}\pi Y_i R \tag{11}$$

where ν_i is the Poisson's ratio of the ith entity. The yield stress of the stainless steel balls is set at 345×10^6 Pa, whereas the yield stress of the Perspex wall is set at 75.9×10^6 Pa. The Poisson's ratio of the Perspex wall is given as 0.35, and the Poisson's ratio of the balls is given as 0.3. These values were simply read off from data handbooks.

The normal viscous damping is set as

$$c_{ni} = 2\zeta\sqrt{k_n m^*} \tag{12}$$

where ζ is the critical damping ratio (a function of contacts, not of entities) and k_n is the effective normal stiffness of the two contacting bodies. For a ball–wall contact, m^* is simply the mass of the ball, whereas for a ball–ball contact, it is given as

$$\frac{1}{m^*} = \frac{1}{m_1} + \frac{1}{m_2} \tag{13}$$

where the ball mass is 0.110 g.

The shear viscous damping follows a similar formulation. Shear viscous damping is, however, not implemented here. The coefficient of restitution α for the contacts between the stainless steel balls and the contacts between the stainless steel balls with the Perspex wall is set at 0.92. This relates to the critical damping ratio by the equation

$$\zeta = \frac{\ell_n(\alpha)}{\sqrt{\ell_n{}^2(\alpha) + \pi^2}} \tag{14}$$

This is basically an averaged value for different operating conditions, as found in experiments described in [6].

The force caused by the Coulomb slider is defined by

$$F_{\text{Coulomb}} = \mu F_n \tag{15}$$

where μ is the coefficient of friction and F_n is the normal force acting on the particle. The coefficient of friction is set at 0.4 for all the

contacts between the Perspex wall and the stainless steel ball bearings, and also between the balls. This was also an averaged value measured from various operating conditions [6]. The only missing ingredient to construct the model is the characterization of the foam.

B. Foam Characterization

The PU foam is a viscoelastic material. Therefore, it will naturally have an energy storage mechanism and an energy dissipation mechanism. To simplify the modeling process, the energy dissipated by the foam is considered negligible compared to the energy lost by the interactions of the particles. Therefore, the stress relaxation time is short compared to the time between each impact the particle agglomerates make on the viscoelastic material. In this way, the particles are assumed to be in contact with the foam at all times. The shear interaction of the foam wall to the particles is also neglected.

By neglecting the energy dissipation of the foam and the shear interactions, the only property that needs to be measured is the compression-force-displacement curve of the foam. To replicate the exact conditions of the power measurement experiments, measurements were performed while the foam was placed on top of a layer of particles in the particle damper casing. The experimental setup is shown in Fig. 8.

Basically, the hydraulic press compresses the foam by 5 mm (50% strain) within 5 min. The force and displacement is acquired in real time while the compression is ongoing. The foam is then taken out of the damper casing and allowed to relax for an unspecified few minutes. The test is then repeated again as desired. Figure 9 shows the force-displacement curve of three such tests.

It can be seen that the curves are close together, although they do not coincide. This is due to the viscous portion of the viscoelastic material. Nevertheless, we will use the averaged value of the three curves as the force-displacement characteristic of the foam in the model. A least-squares fit is performed through this averaged curve with a cubic polynomial.

Foams under compression usually go through four phases. The first phase is when the walls are still holding, the second phase is when some of the walls have started buckling, the third phase is when the buckled walls start to touch one another, and the last phase is when all the walls have buckled and are touching one another [11]. This behavior usually manifests itself in an almost cubic curve, which is why a cubic polynomial was chosen to fit the curve.

The average number of balls in the top layer that is in contact with the foam is 75. Therefore, the force that is acting on each particle in the simulation is calculated as a function of the cubic polynomial divided by 75. This is given by

$$F_{\text{foam}}(\delta) = 4.35 \times 10^5(\delta + \delta_c)^3 - 2.73 \times 10^3(\delta + \delta_c)^2 + 12.48(\delta + \delta_c) \tag{16}$$

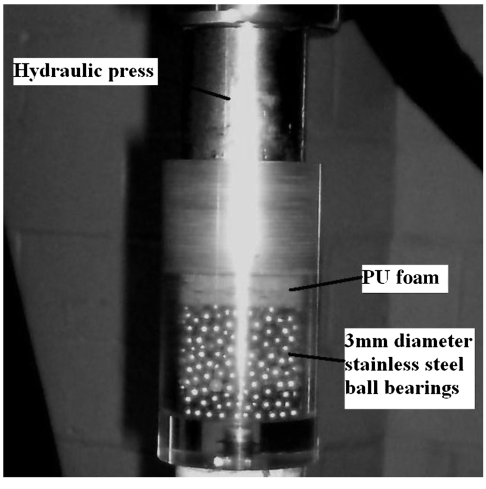

Fig. 8 Rig used to measure stiffness of PU foam.

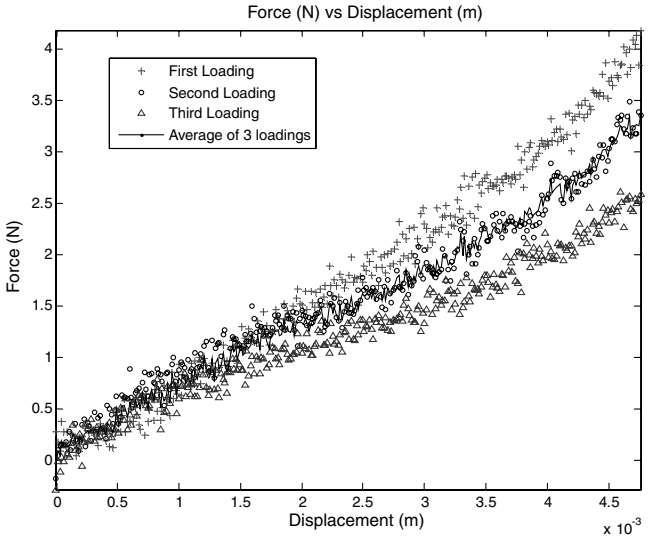

Fig. 9 PU foam force-displacement curve. Data have been downsampled by a factor of 100 for the purposes of illustration clarity.

where δ is the depth of penetration the particle has passed through the initial foam wall position and δ_c is the amount of displacement the foam has been compressed statically by the Perspex wall above.

C. Simulation Implementation

Having all the required parameters for the modeling process, models of the damper can now be created. First, the Perspex walls are created. Particles are then randomly generated within the walls. The particles are then allowed to fall from gravity loading and to settle within 60,000 time steps. The positions of all the particles are then recorded; it will be loaded up for each subsequent run to speed up the simulation process. Ideally, we would like to use the built-in wall functions in PFC3D 3.1 to represent the PU foam. Unfortunately, this is plagued by a number of issues. First of all, if an equivalent linear wall was built, the initial stiffness as the ball is touching the wall is nearly negligible. When the ball that is passing through the wall has a high inertial force, it can possibly penetrate through the wall. PFC3D 3.1 does not detect any contacts when the center point of the particle passed through an active side of the wall (the active side is defined during wall creation; it basically specifies the side of the wall that the ball can have contact with). This might have been resolved by using a much stiffer wall, and then moving the wall to compensate for the additional force for a certain displacement. However, PFC3D assumes that the walls do not warp. This is important as the foam is touching the top layer of the particles at all times. A nonwarping wall cannot touch all the particles in the top layer at all times, unless all the particles move together at the same rate (which cannot be guaranteed).

A simpler solution was arrived at to solve this problem. A virtual boundary is created at 9 mm above the bottom of the Perspex wall casing. A Perspex wall is included above this virtual boundary as well, reproducing the same conditions as the physical experiments. During excitation of the walls of the damper, the algorithm searches for the top 75 particles in terms of its position in the z axis (marked as the black balls in Fig. 10) at every time step of the simulation. These particles will represent the particles at the top layer of the particle assembly. A body force is then applied to these particles based on Eq. (14), depending on how much the particles have penetrated through the virtual boundary. This method removes the spring and viscous damper contacts formulation between the foam wall and the particles. This is acceptable and is in fact justified for a few reasons.

First, the force approximation already takes into account the effective stiffness of the particles–foam-wall contacts. Therefore, no equation is needed to characterize the stiffness of the wall individually. The shear interactions between the foam and the Perspex wall have also been accounted for. The viscous damper contact actually represents energy dissipation caused by plasticity in

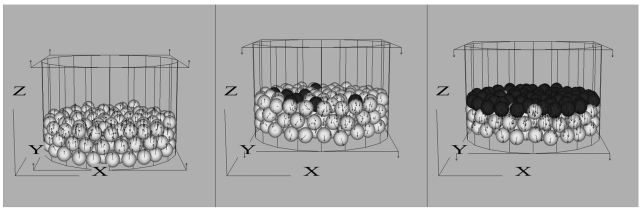

Fig. 10 Particle damper at various stages of vibration. This simulation was at 25 Hz and 5 g for the uncompressed foam configuration. The black balls represent the top layer that is touching the foam.

the material when it is deformed. It is thought that the cushioning effect of the foam will actually make it difficult for plastic deformations for the contacts between the foam wall and the particles. Therefore, the viscous damper contacts would have to be removed anyway. There is no shear interaction between the particles and the foam wall. This is mainly because there is not enough information at the moment about foam and particle shear interactions, and it would have complicated the simulations.

The walls are then excited in a sinusoidal fashion, corresponding to the physical experiment settings. The number of operating points, however, has been reduced by half for the frequency dimension and also for the amplitude dimension. This is to reduce the simulation time. Each of the operating points were simulated for 40,000 time steps. The accumulated work done by the walls is calculated at every time step with the assumption that the force is constant at every time step. Because of the energy balance, the steady-state work done by the Perspex walls and the foam is equivalent to the energy dissipated by damping. Twenty-thousand time steps of work done by the walls were recorded (by downsampling the 40,000 time steps to reduce storage space) at the end of each run. The first 2000 time steps of the energy trace recorded were deleted to remove the transients. The remaining values were then used to estimate the power dissipation by fitting a linear model to the time history.

The power dissipation calculated from the experiments is shown in Fig. 11. Despite the simplifications made, the simulations have managed to capture the exact same trends as those measured from the experiments. The peak of power dissipation is at the same position as that measured from the experiments. It can also be seen that the peak shifts toward the higher frequencies as the foam is compressed. The power dissipated also spreads out over a wider range of frequencies. Nevertheless, it is noted that the absolute values of the power dissipated were lower than that measured from the experiments. In most cases, the values were between 25–30% lower, except for the configuration where the foam has been compressed by 6 mm. These discrepancies can be explained somewhat by some of the gross simplifications made in selecting some of the material and contact parameters. This was also discussed in [10].

The other issue is the problem of modeling the foam wall. Energy dissipation of the viscoelastic foam was not considered to be important. It is, however, possible that it does dissipate quite a significant portion of energy away. This includes dissipation when the foam is undergoing compression and also when the particles are rubbing against the bottom of the foam wall (leading to energy lost by friction). The elastic compressive force of the foam wall was also crudely measured by not considering the energy dissipation as well. This could be seen in the different loading curves when it was loaded at different times. Previous material tests done on the foam yielded a loss factor of approximately 0.1 for the range of frequencies between 20–200 Hz and of low dynamic strain up to 1×10^{-3}. Although these material tests were performed in a different configuration than that of the particle damper, it will provide a very crude idea of how much energy dissipation is accounted for by the foam. By linearizing the stiffness of the nonlinear foam for different dynamic displacements [based on the strain energy of the foam calculated from Eq. (16) and assuming the stiffness does not change with frequency] and extracting the penetration distance of the balls into the foam wall (from simulations), an approximation of power dissipated by the foam can be calculated (assuming a constant loss factor of 0.1):

$$P_{\text{foam}} = 0.0125 k_{\text{foam}} \omega \delta^2 \tag{17}$$

where k_{foam} is the linearized stiffness of the wall foam (650–920 N/m). Assuming that the power dissipation characteristics of the foam do not change with preloading, the foam contributes to roughly an additional 7–10% increment in the power dissipation for most operating and preloading conditions. The only exceptions to this are those at 25 Hz, where it was found that the foam contributed nearly an extra 60–200% in terms of power dissipation. One of the root causes of this anomaly is due to the fact that the penetration distance calculated from the simulation for 25 Hz is beyond the thickness of the foam itself. Despite this, it does partially explain the lower power dissipation calculated from the simulations as compared to the experiments. Nevertheless, a more complete dynamic characterization of the foam is needed to provide a more

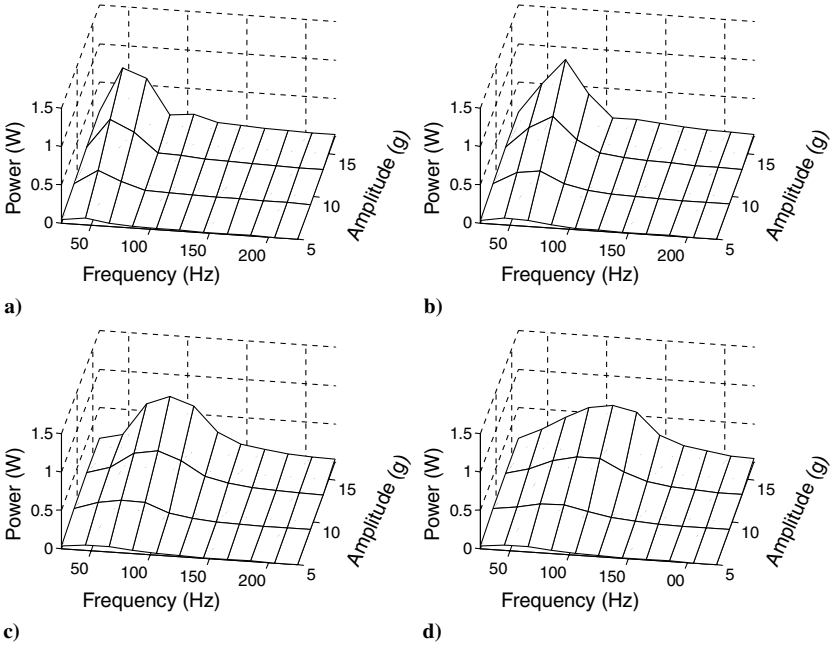

Fig. 11 Power dissipated calculated from DEM models for a) uncompressed foam, b) foam compressed by 1.5 mm, c) foam compressed by 4 mm, and d) foam compressed by 6 mm.

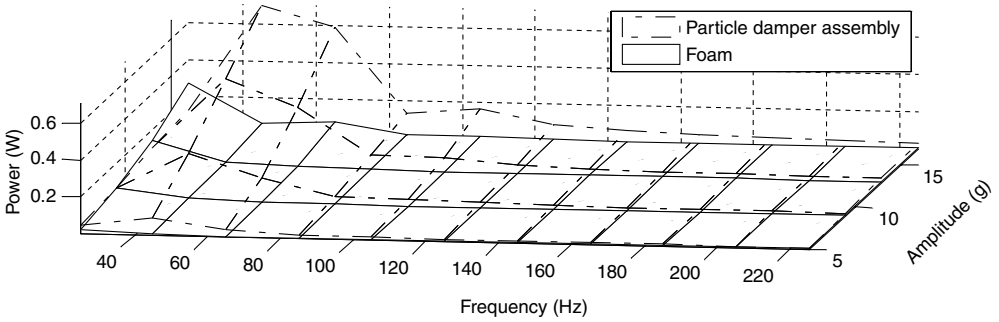

Fig. 12 Power dissipated calculated from DEM models for uncompressed foam configuration and power dissipated by the foam itself.

conclusive answer. A plot of the comparison between the power dissipated by the uncompressed foam wall particle damper configuration (simulated) and power dissipated by the foam is shown in Fig. 12.

Apart from not limiting the foam wall penetration distance, there are other issues that have not been addressed in the simulation. First of all, it is not known whether the foam wall is actually touching 75 balls at all times. It was also not possible to tell where the virtual boundary should be exactly in all the configurations. It was chosen as 9 mm above the bottom Perspex wall simply because that was the height of the highest ball within the particle damper. In fact, a quick inspection of Fig. 10 shows that the balls marked for the application of body forces may not cover all the balls at the top layer. The effective mass of the system has not been calculated from the simulations as well. The effective mass and the other problems related to the energy dissipation of the foam will be explored further in future works.

IV. Conclusions

The work reported in this paper aimed at finding more ways to better control the performance of a particle damper. The results of this paper have shown it is indeed possible to control it by constraining the movement of the particles with a pressure boundary. The pressure boundary in this case is introduced by the PU foam with a nonlinear stiffness. This configuration actually adds another extra level of dynamic, where it actually resembles a tuned mass damper (with the foam acting as a tunable spring and the particle assembly as the mass), except that extra levels of damping are occurring within the foam and the particle assembly. It is a simple configuration that is indeed worth further exploration.

The DEM technique used also found good correlation with the power dissipation calculated from an experiment. However, there are some issues with the measurements and simulations that have been discussed in the paper. One way to reduce the severity of these issues is to perform a sensitivity and uncertainty analysis of the different parameters. This will at least allow us to concentrate our efforts on the correct issues; material and contact parameters that do not affect the output much can be measured with crude methods with impunity. We have also yet to use DEM to measure the effective mass of particle dampers. This is also an important parameter that is needed to characterize vibration suppression.

Once the modeling is further refined, we can experiment with various configurations. It will be interesting to attempt to optimize the damper with a combination of other particle damper control methods (e.g., electromagnetic fields, geometry modification). This would allow rapid prototyping of particle dampers while minimizing testing in the lab and the cost of manufacturing prototypes. Needless to say, despite all these advancements in computational and theoretical understanding, work so far has barely scratched the surface of the subject of granular media and its role in particle damping. The potential for particle damping is indeed a promising one in various applications. A significant next step is to demonstrate a complete framework for designing and applying particle dampers in applications accurately in the future.

Acknowledgments

C. X. Wong is funded by Engineering and Physical Sciences Research Council contract EP/D078601/1. The authors are grateful for the help extended by Dave Webster and Leslie Morton in setting up the experiments.

References

[1] Liu, W., Tomlinson, G. R., and Rongong, J. A., "The Dynamic Characterisation of Disc Geometry Particle Dampers," *Journal of Sound and Vibration*, Vol. 280, Nos. 3–5, 2005, pp. 849–861. doi:10.1016/j.jsv.2003.12.047

[2] Rongong, J. A., and Tomlinson, G. R., "Amplitude Dependent Behaviour in the Application of Particle Dampers to Vibrating Structures," AIAA Paper No. 2327, 2005.

[3] Saluena, C., Esipov, S. E., Poschel, T., and Simonian, S., "Dissipative Properties of Granular Ensembles," *SPIE Proceedings*, 3327, Society of Photo-Optical Instrumentation Engineers, Bellingham, WA, 1998, pp. 23–29.

[4] Saluena, C., Poschel, T., and Espiov, S. E., "Dissipative Properties Of Granular Materials," *Physical Review E (Statistical Physics, Plasmas, Fluids, and Related Interdisciplinary Topics)*, Vol. 59, No. 4, 1999, pp. 4422–4425. doi:10.1103/PhysRevE.59.4422

[5] Yang, M. Y., "Development of Master Design Curves for Particle Impact Dampers," Ph.D. Thesis, Pennsylvania State Univ., University Park, PA, 2003.

[6] Wong, C. X., Daniel, M. C., and Rongong, J. A., "Prediction of the Amplitude Dependent Behaviour of Particle Dampers," AIAA Paper No. 2043, 2007.

[7] Popplewell, N., and Semercigil, S. E., "Performance of a Beam Bag Damper for a Sinusoidal External Force," *Journal of Sound and Vibration*, Vol. 133, No. 2, 1989, pp. 193–223. doi:10.1016/0022-460X(89)90922-X

[8] Particle Flow Code in 3 Dimensions, Software Package, Ver. 3.1, Itasca Consulting Group, Minneapolis, MN, 2005.

[9] Universal Distinct Element Code, Ver. 4.0., Itasca Consulting Group, Minneapolis, MN, 2004.

[10] Wong, C. X., Daniel, M. C., and Rongong, J. A., "Energy Dissipation Prediction of Particle Dampers," *Journal of Sound and Vibration*, Vol. 319, Nos. 1–2, 2009, pp. 91–118. doi:10.1016/j.jsv.2008.06.027

[11] Mills, N. J., "Micromechanics of Polymeric Foams," *Proceedings of the 3rd Nordic Meeting on Materials and Mechanics*, Inst. of Mechanical Engineering, Aalborg Univ., Aalborg, Denmark, 2000, pp. 45–76.

J. Cooper
Associate Editor